Website : jurnal.umj.ac.id/index.php/icecream

Numerical Prediction of Shell and Tube Heat Exchangers Performance with Fold Segmental Baffle

Widyastutifajri Nuha[1], Joko Waluyo[1*], and Indro Pranoto[1]

[1]Department of Mechanical and Industrial Engineering, Faculty of Engineering, Gadjah Mada University, Jl. Grafika No. 2 Kampus UGM, Yogyakarta 55281, Indonesia.
**Email address of corresponding author: jokowaluyo@ugm.ac.id*

ABSTRACT

Shell and Tube Heat Exchanger (STHE) has been used widely used in industry for energy transferring between two and more fluids. Effectiveness of STHE is enhanced by utilizing baffle on the fluid passage in the shell. In this research, a novel baffle which has specific geometrical shape is investigated. The baffle is built based on segmental baffle which is fold on the edge with variation fold angel 120˚, 135˚, and 150˚. This research is carried out using numerical simulation with ANSYS, and validated using experimental data. This research compares conventional and fold segmental baffles performance on the shell and tube heat exchanger. Research revealed that the 150˚-fold angle has superior performance as indicated by the highest effectiveness (ε) among the fold segmental baffle. For comparison, at a mass flow rate of the fluid in shell of 0.4 kg/s, the effectiveness is obtained at 31.521%; 31.077%, 31.764%, and 31. 928% for conventional segmental baffle, fold angle 120˚, 135˚, and 150˚, respectively. In addition, the pressure drops of the fold segmental have no significant difference with that on the conventional segmental baffle. Comparing between the conventional and fold segmental baffle, it is noted that fold segmental baffle offers better performance, especially fold angle of 135º and 150º. This finding offer prospectus advantage of using fold segmental baffle in shell and tube heat exchanger.

Keywords : CFD, effectiveness, heat transfer coefficient, segmental baffle, shell and tube heat exchanger.

1. Introduction

A heat exchanger is a device used to efficiently transfer heat between two fluids (gas or liquid). Using heat exchangers in a system can improve thermal control and save energy. Shell and Tube Heat Exchanger (STHE) is a type of heat exchanger that has been widely used in various industries, such as power plants, chemical industry, petroleum refining, and waste heat utilization [1]. STHE are almost installed baffle on the fluid passage in the shell.

Configuration of geometrical shape has significant role on the performance of STHE, therefore it has been subjected by researcher. Experimental research of baffle in the STHE has been carried out El-Said [2], and Yogiswara [3]. El-Said [2] conducted experimental research using four types of segmental baffle configurations, namely conventional single segmental baffle (CSSB), staggered single segmental baffle (SSSB), flower segmental baffle (FSB) and hybrid segmental baffle (HSB). In this study HSB is a type of baffle with the best thermal performance and effectiveness compared to the others. Yogiswara [3] conducted experimental research on the effect of baffle type and mass flow rate ratio in heat transfer rate to pressure drop in a vertical shell and tube condenser. This study uses four types of baffles: segmental baffle, disc and doughnut baffle, three-quarter baffle 90˚ configuration, and three-quarter baffle 180˚ configuration. At mass flow rate ratios of 3.24 and 3.6, the three-quarter baffle 90˚ configuration provides the most significant ratio of the difference in heat transfer rate to pressure drop, namely 0.96 and 1.28. However, at a mass flow rate ratio of 3.96, the value of the ratio of the difference in the heat transfer rate to the highest-pressure drop is obtained in the three-quarter baffle 180˚ configuration.

Numerical simulations have also been investigated by Lei [4], Marzouk [5], Abbasi [6], and Wang [7]. Lei [4] researched the effect of using louver baffles compared to segmental

baffles on the heat transfer coefficient in STHE using computational fluid dynamics. Louver baffles were made in two configurations, namely STHX-LV1 (with three inclined plates on one baffle ring) and STHX-LV2 (with three inclined plates and two inclined plates on another baffle ring). The results showed that the heat transfer coefficient per pressure drop on STHX-LV1 has the best overall performance among the three baffle variations in the heat exchanger.

Marzouk [5] conducted research by varying the baffle model, namely conventional single segmental (CSS), staggered single segmental (SSS), flower segmental (FS), hybrid segmental (HS), circular ring (CR), and circular ring with holes (CRH) through CFD simulation. The results of this study show that CRH provides the best thermal performance compared to other baffle types. Abbasi [6] researched the effect of baffle angles (45°, 90°, and 135°) using porous materials simulated with CFD and analyzed them using Artificial Neural Network (ANN). Increasing the baffle angle from 45˚ to 135˚ (in the configuration of Nb = 6 and b = 5 mm) caused a decrease in the heat transfer rate by 36.8% and significantly affected the pressure drop by 80.9%. Wang [7] investigated the effect of helical baffle fold angle on Nusselt Number (β). The baffle fold angles used in this study are 18˚, 29˚, and 40˚. The results of this study also show that the Nusselt Number has a negative correlation with an increase in the baffle fold angle. The smallest baffle fold angle of 18˚ gives the most considerable Nusselt number value [8].

This research is focused on numerical prediction of a novel baffle layout with a novel geometrical shape. The baffle is constructed using a segmental baffle which is fold at the edge 120˚, 135˚, and 150˚. Numerical simulation is used in this investigation, after being validated with experiment data.

2. Material and Methods

The research methodology involves several steps starting with data collection and 3D STHE design. The data is then used to model the fluid domain, followed by the meshing process. From the meshing results, input parameters were set up in the CFD software, and numerical simulations were performed. Validation of the simulation results is done by comparing them with experimental data with an error below 10%. After the results are accepted valid, then proceed with conducting numerical simulations to each type baffle model with mass flow rate variations. The mass flow rate at the shell and tube inlet is set constant. The mass flow rate is set at 0.2 kg/s on the tube side. On the shell side, the mass flow rate are varied at 0.2 kg/s, 0.3 kg/s, and 0.4 kg/s vary.

2.1. STHE Specification

The initial step in the simulation process is to create a 3D model geometry of the fluid domain simulated with variations in the baffle fold angle model. The STHE specifications are shown in Table 1, and the STHE fluid domain model used in this study is shown in Figure 1. The fluid domain design process uses Autodesk Inventor Professional 2020 software and is then integrated into ANSYS Design Modeler.

Table 1: STHE Specifications

Item	Dimensions and description
***Shell*-side parameters**	
Inner diameter (mm)	200
Thickness (mm)	2.5
***Tube* parameters**	
Outer diameter (mm)	19
Thickness (mm)	1.5
Effective length (mm)	1000
Number	32
Tube pitch (mm)	28.5
***Baffle* parameters**	
Cut ratio (%)	20
Thickness (mm)	1.5
Number	6
Baffle pitch (mm)	142

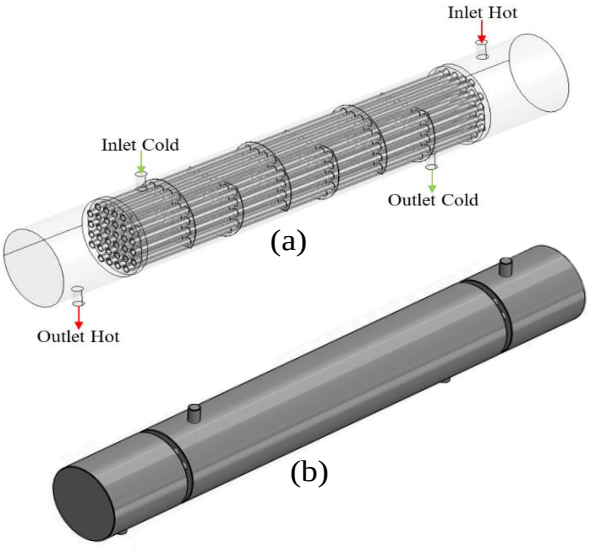

Figure 1: Shell and Tube Heat Exchanger (a) 3D Model (b) 3D Fluid Domain

The working fluid passing through the shell and tube in this study uses water. Data on the

properties of the fluid passing through the shell and tube are shown in Table 2.

Table 2: Fluid Properties

Properties	Symbols	Values
Fluid in Shell		
Temperature *inlet*	T_1	28 ˚C
Density	ρ	996,26 kg/m^3
Thermal conductivity	k	0,5997 W/m.K
Specific heat	c_p	4183 kJ/kg.K
Dynamic viscosity	μ	0,000835 Pa.s
Fluid in Shell		
Temperature *inlet*	t_1	82 ˚C
Density	ρ	970,52 kg/m^3
Thermal conductivity	k	0,6573W/m.K
Specific heat	c_p	4196 kJ/kg.K
Dynamic viscosity	μ	0,000346 Pa.s

2.2. Baffle Model

This study used four baffle models, namely the conventional segmental baffle and three fold segmental baffle modification models, as shown in Figure 2. The segmental baffle modification was folded at various angles, namely 150˚ angle (S-150), 135˚ angle (S-135), and 120˚ angle (S-120).

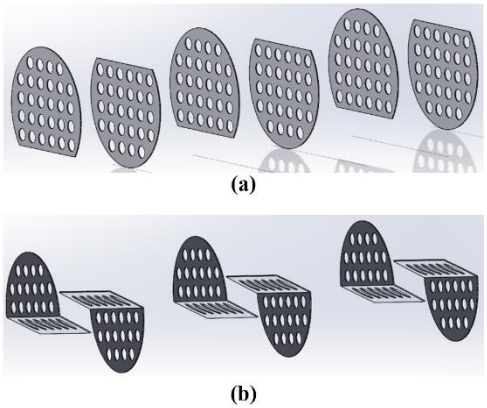

Figure 2: (a) Segmental Baffle and (b) Modified Fold Segmental Baffle

2.3. Modeling Equation Simulation

The simulation uses Reynolds-Averaged Navier-Stokes (RANS) equations that contain equations governing continuity, momentum, and energy. The governing equation is written as follows [5] [10]:

$$\frac{\partial}{\partial x_i}(\rho u_i) = 0 \tag{1}$$

$$\frac{\partial}{\partial x_i}(\rho u_i u_k) = \frac{\partial \rho}{\partial x_i} + \frac{\partial}{\partial x_i}\left(\mu \frac{\partial u_k}{\partial x_i}\right) \tag{2}$$

$$\frac{\partial}{\partial x_i}(\rho u_i T) = \frac{\partial}{\partial x_i}\left(\mu \frac{\partial T}{\partial x_i}\frac{K}{C_P}\right) \tag{3}$$

The realizable k-ε model is employed. The governing equations for this particular model are as follows [11]:

$$\frac{\partial}{\partial t}(\rho k) + \frac{\partial}{\partial x_j}(\rho k u_j) = \frac{\partial}{\partial x_j}\left[\left(\mu + \frac{\mu_t}{\sigma_k}\right)\frac{\partial k}{\partial x_j}\right] + G_k + G_b - \rho\varepsilon - Y_M + S_k \tag{4}$$

$$\frac{\partial}{\partial t}(\rho \varepsilon) + \frac{\partial}{\partial x_j}(\rho \varepsilon u_j) = \frac{\partial}{\partial x_j}\left[\left(\mu + \frac{\mu_t}{\sigma_\varepsilon}\right)\frac{\partial \varepsilon}{\partial x_j}\right] + \rho C_1 S\varepsilon - \rho C_2 \frac{\varepsilon^2}{k + \sqrt{\nu\varepsilon}} + C_{1\varepsilon}\frac{\epsilon}{k} C_{3\varepsilon} G_b + S_\varepsilon \tag{5}$$

$$C_1 = max\left[0.43, \frac{\eta}{\eta + 5}\right], \eta = S\frac{k}{\varepsilon}, S = 2\sqrt{2S_{ij}S_{ij}} \tag{6}$$

2.4. Performance of STHE

Characterization of the STHE performances are carried out using several parameters : log mean temperature difference (ΔTLM), heat transfer rate ($\dot{Q}$), overall heat transfer coefficient (U), and effectiveness (ε). The calculation of each parameter is written as follows [5] [10]:

$$\Delta T_{LM} = LMTD = \frac{(T_{h,out} - T_{c,out}) - (T_{h,in} - T_{c,in})}{\ln \frac{(T_{h,out} - T_{c,out})}{(T_{h,in} - T_{c,in})}} \tag{7}$$

$$\dot{Q} = \dot{m} \cdot c_p \cdot \Delta T \tag{8}$$

$$U = \frac{U\,A}{(\dot{m}_c c_p)_{minimum}} \tag{9}$$

$$NTU = \frac{\dot{Q}}{A\,\Delta T_{LM}} \tag{10}$$

$$\varepsilon = \frac{\dot{m}_c c_{p,c}\,(T_{c,out} - T_{c,in})}{(\dot{m}_c c_{p,c})_{minimum}\,(T_{h,in} - T_{c,in})} \tag{11}$$

2.5. Experimental Set-Up

This research is initially settled with experimental works. The obtained data from the

experiment is used to validate the simulation model. The simulation, is therefore uses the same configuration on the STHE, working mass flow rate, as well as its boundary conditions are set to be the same as those set in the simulation. In the experimental, the mass flow rate at the inlet shell and tube is set constant. The mass flow rate at inlet shell are varied to 0.283, 0.216, and 0.349 kg/s. Meanwhile, at the inlet tube, the mass flow rate is set at 0.128 kg/s. The experimental equipment setup is shown in Figure 3.

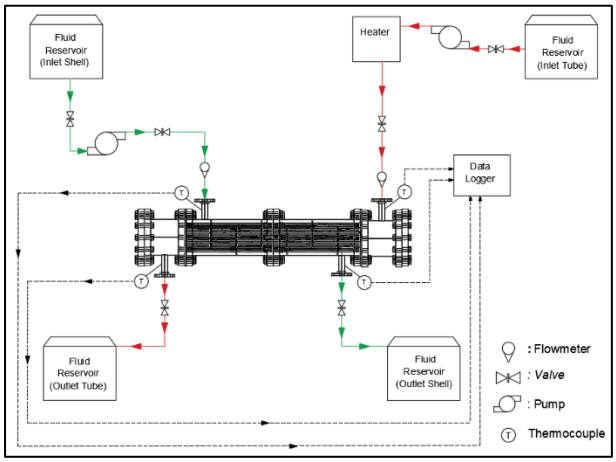

Figure 3: Experimental Set Up

3. Results and Discussions

3.1. Meshing

The mesh types used in this study are Tetrahedral and Hexahedral. The number of meshes used in this study is 6.897x 10^6 with a skewness value of 0. 24001, which is in the very good range, and an orthogonal quality value of 0.75607, which is in the very good range [12]. The skewness and orthogonal quality values show that the fluid domain model used is good enough. This meshing process uses ANSYS Meshing.

3.2. Convergence

In this study, convergence criteria are used to determine when the numerical simulation is considered to have converged. For the continuity equation, the convergence criterion is an accuracy of 10^{-2}. This means that the difference between the actual value and the previous iteration's value must be less than 10-2 to ensure mass conservation is adequately met. For the energy equation, the convergence criterion is set at 10^{-5}. Other parameters, such as velocity, pressure, or turbulence, have a convergence criterion of 10^{-3}. In this study, the numerical simulation successfully achieved convergence at the 536th iteration, indicating that the simulation results have been stable and reliable for further analysis.

3.3. Validation

The simulation results obtained from the conventional segmental baffle model were validated by comparing the output temperature values on the shell and tube sides. The comparison between the two parameters is shown in Table 3. The results of the simulation and experimental shell and tube outlet temperature comparison all show values below 10%. This shows that the simulation method can be accepted as valid.

Table 3: Validation with experimental and simulation results

Mass Flow Rate (kg/s)	Outlet Shell Temperature			Outlet Tube Temperature		
	Experiment	Simulation	Deviation (%)	Experiment	Simulation	Deviation (%)
0,283	32.12	30.678	4.49	40.14	40.86	1.76
0,316	33.20	30.582	7.89	41.46	41.33	0.32
0,349	33.85	30.470	9.99	43.35	41.24	4.87

3.4. Temperature Distribution

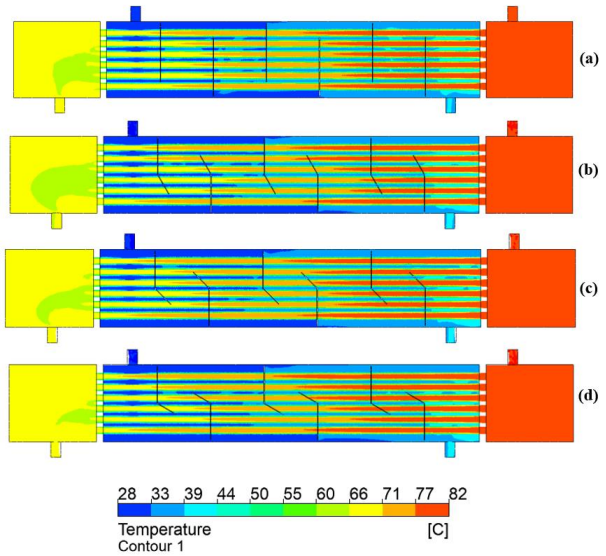

Figure 4: Temperature Distribution in STHE with (a) conventional Segmental Baffle, (b) S-150, (c) S-135, and (d) S-120.

The temperature distribution for the four baffle models is shown in Figure 4. It can be observed that STHE with conventional segmental baffle has uniform temperature in the area close to shell outlet and also the tube outlet as shown in Figure 4(a). Meanwhile, The S-150 baffle in Figure 4(b) shows a larger area of fluid

temperature reduction when approaching the shell outlet. The use of the S-150 baffle causes the fluid temperature on the shell side has uniform distribution and the hot fluid temperature has a lower temperature compare to the others. Figure 4(c) shows the temperature distribution of STHE with the S-135 baffle, on the shell side the temperature distribution of the S-135 model is less uniform compared to the S-150 baffle and the area of fluid temperature decrease at the outlet tube is also smaller than the S-150 baffle. Figure 4(d) gives a smaller area of temperature drop in the area close to the shell outlet and on the outlet tube side the temperature distribution is less spread unevenly.

3.5. Pressure Distribution

Pressure distribution in STHE with various baffle models is shown in Figure 5. It is shown at Figure 5(a), 5(b), 5(c), 5(d) for conventional segmental, fold angle of 150^o, 135^o, 120^o, respectively. The area around the shell inlet and inlet tube shows relatively has the same pressure as the area inside the shell, the pressure then decreases when entering the shell outlet area.

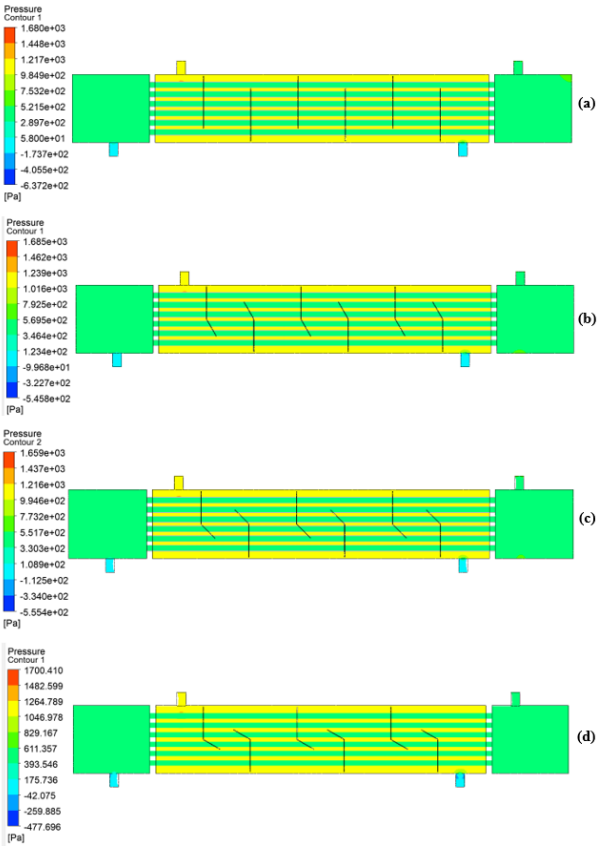

Figure 5: Pressure Distribution in STHE with (a) Segmental Baffle, (b) S-150, (c) S-135, and (d) S-120.

At the tube side, the tube inlet has similar pressure pattern for all models. The pressure is also relatively the same and then decreases drastically at the outlet tube area, this phenomena are occurred in all baffle models. The four baffle models show the same pattern of pressure distribution in the simulations, this indicates that the pressure distribution among the models has no significant difference.

3.6. Velocity Distribution

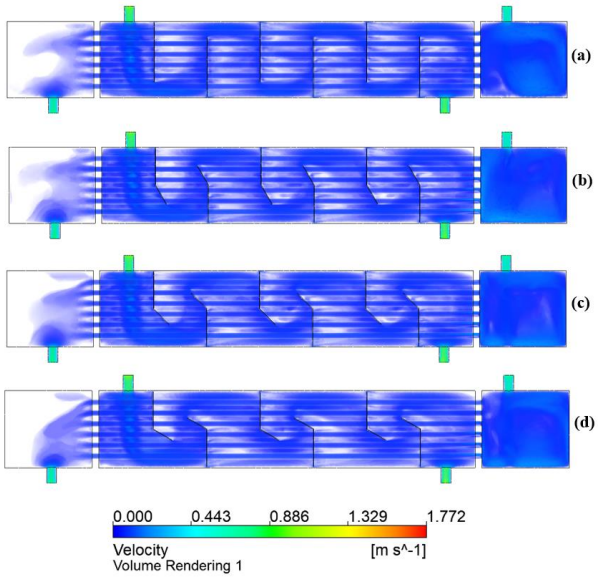

Figure 6: Velocity Distribution in STHE with (a) Segmental Baffle, (b) S-150, (c) S-135, and (d) S-120.

The velocity distribution passing through the segmental baffle in Figure 6(a) causes the formation of a dead zone around the baffle. This dead zone has an impact on reducing the effectiveness of heat transfer. Folding the baffle causes the fluid flow pattern passing through the shell to be deflected. In Figure 6(b) the S-150 baffle model shows a narrow dead zone space behind the baffle, then causes increase fluid contact with the surface, so that increases the heat transfer effectiveness.

In the case of the S-135 baffle model in Figure 6(c), S-135 has also shown the similar dead zone formation. The dead zone difference among the models occurred on its intensity and density. However, the S-135 baffle results in a larger dead zone in the area in front of the baffle compared to the S-150 baffle model, which leads to an increase in heat transfer effectiveness but is not so optimal.

The velocity distribution of the fluid flow passing through baffle S-120 is shown in Figure 6(d). In baffle S-120, it can be observed that this baffle produces a smaller dead zone in the

area behind the baffle, but the large open area in front of the baffle also causes the formation of a wider dead zone compared to other models. This large dead zone results in a limited contact area between the fluid and the baffle surface, thus reducing the ability of the baffle to transfer heat effectively.

3.7. Performances of STHE

Figure 7 shows the impact of various mass flow rates (0.2 kg/s, 0.3 kg/s, and 0.4 kg/s) on the shell side on the overall heat transfer coefficient (U) of the four baffle models used.

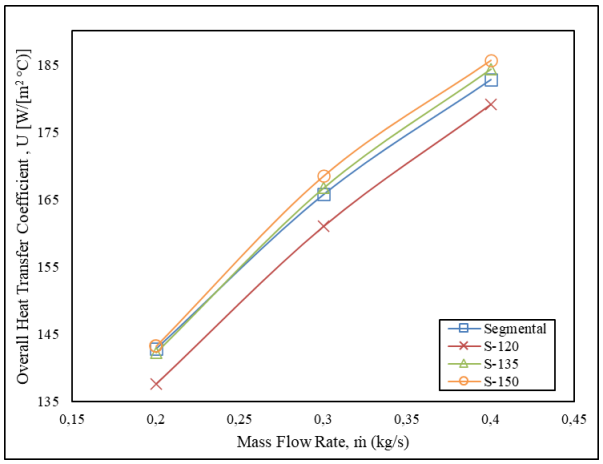

Figure 7: Overall Heat Transfer Coefficient vs. Mass Flow Rate on Shell Side

The overall heat transfer coefficient (U) consistently increases with the rise in mass flow rate in all baffle models. The S-150 baffle model yields the highest overall heat transfer coefficient (U), while the lowest overall heat transfer coefficient value was observed at the S-125 baffle model. The highest overall heat transfer coefficient was obtained at a mass flow rate of 0.4 kg/s 4 in all four baffle models: S-120, S-135, S-150, and segment baffles respectively, with values of 179.114 W/(m².˚C), 184.393 W/(m².˚C), 185.634 W/(m².˚C), and 182.781 W/(m².˚C), respectively.

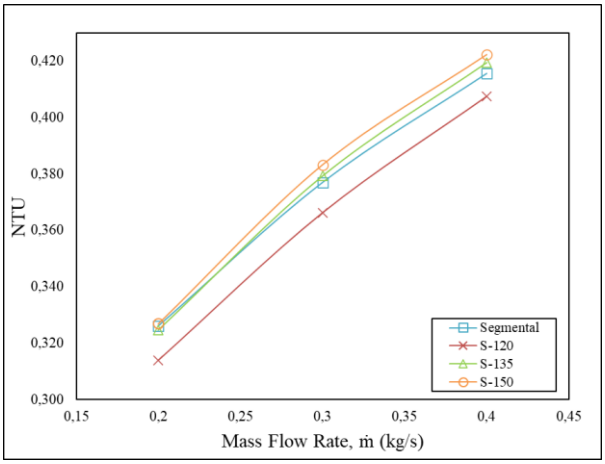

Figure 8: NTU vs. Mass Flow Rate on Shell Side

The effect of mass flow rate variations on the Number of Transfer Units (NTU) is depicted in Figure 8. The NTU values consistently increase with an increase in mass flow rate, a trend observed across all baffle models utilized. The S-125 baffle model presents the lowest NTU values at each mass flow rate, whereas the S-150 baffle model exhibits the highest NTU values compared to the other models. The highest NTU value was obtained at a mass flow rate of 0.4 kg/s in all simulated baffle models namely S-120, S-135, S-150, and conventional segmental baffles with NTU values of 0.407, 0.419, 0.422, and 0.416, respectively.

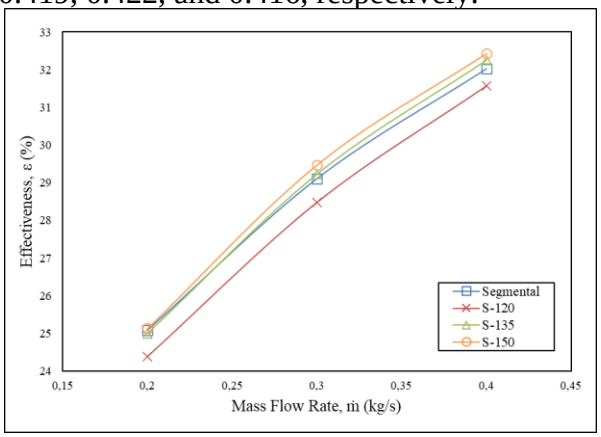

Figure 9: Effectiveness vs. Mass Flow Rate on Shell Side

The chart showing the impact of mass flow rate variations on effectiveness is presented in Figure 9. The trend depicted by the graph showing increase in effectiveness values corresponding to the rise in mass flow rates, this applies to the four baffle models used. The S-150 baffle model obtained the highest effectiveness. The highest effectiveness is obtained at a mass flow rate of 0.4 in all four baffle models: S-120, S-135, S-150, and

segment baffles respectively, with effectiveness values of 31.077%, 31.764%, 31.928%, and 31.521%.

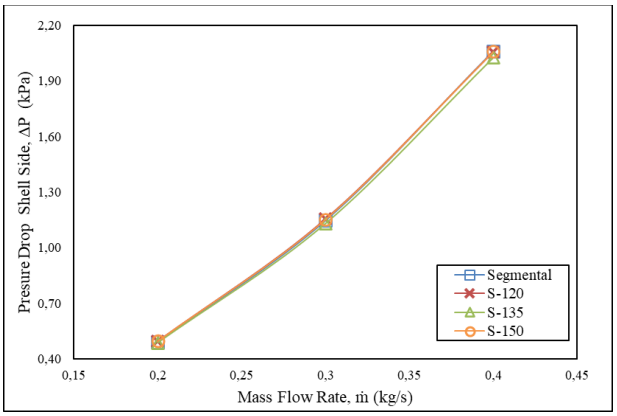

Figure 9: Pressure Drop Shell Side vs. Mass Flow Rate on Shell Side

Figure 10 presents a correlation between the values of pressure drop and the variations in mass flow rates. A rising mass flow rate leads to an increase in the pressure drop for each baffle model analyzed. The highest pressure drop in this study was obtained at a mass flow rate of 0.4 kg/s at each baffle, namely S-120, S-135, S-150, and conventional segmental baffles with pressure drop values respectively of 2.058 kPa, 2.025 kPa, 2.056, and 2.062.

4. Conclusion

The research revealed that the fold segmental baffle model showed the most superior performance compare to the other baffle, even compare to segmental baffle.
Pointing results on mass flow rate of 0.4 kg/s fluid on shell side, the effectiveness were obtained at 31.077%; 31.764% and 31.928%, for fold angle baffle of 120^o, 135^o and 150^o. The effectiveness of fold angle 135^o and 150^o are higher compare to that of the segmental baffle, 31.521%. The pressure drop are also investigated. On the pointing results on mass flow rate of 0.4 kg/s fluid on shell side, the pressure drop are obtained at 2.058 kPa; 2.025 kPa and 2.056 kPa, for fold angle baffle of 120^o, 135^o and 150^o. The results also indicates that the pressure drop of 135^o fold angle is lower than that on the conventional segmental baffle 2.062 kPa. It is highlighted that fold segmental baffle is able to reduce the dead zone area in the fluid passages in the shell, that increase the overall effectiveness of the heat exchanger. It is also noted that pressure drop occurred at fold segmental baffle shows no significant different with that on the conventional baffle

Acknowledgement

Financial support provided by the Center for Higher Education Funding (BPPT) and Indonesia Endowment Fund For Education (LPDP).

References

[1] Luo, C., & Song, K. (2021). Thermal performance enhancement of a double-tube heat exchanger with novel twisted annulus formed by counter-twisted oval tubes. *International Journal of Thermal Sciences*, 164, 106892. https://doi.org/10.1016/j.ijthermalsci.2021.106892

[2] El-Said, E. M. S., & Abou Al-Sood, M. M. (2019). Shell and tube heat exchanger with new segmental baffles configurations: A comparative experimental 82 investigation. *Applied Thermal Engineering*, 150, 803–810. https://doi.org/10.1016/j.applthermaleng.2019.01.039

[3] Yogiswara, C. Wibi. (2023). Studi Eksperimental Pengaruh Jenis Baffle dan Rasio Laju Aliran Massa Fluida Pada Kondensor Vertikal Tipe Shell and Tube. Yogyakarta : Universitas Gadjah Mada.

[4] Lei, Y., Li, Y., Jing, S., Song, C., Lyu, Y., & Wang, F. (2017). Design and performance analysis of the novel shell-and-tube heat exchangers with louver baffles. *Applied Thermal Engineering*, 125, 870–879. https://doi.org/10.1016/j.applthermaleng.2017.07.081

[5] Marzouk, S. A., Al-Sood, M. M. A., El-Fakharany, M. K., & El-Said, E. M. S. (2022). A comparative numerical study of shell and multi-tube heat exchanger performance with different baffles configurations. *International Journal of Thermal Sciences*, 179. https://doi.org/10.1016/j.ijthermalsci.2022.107655

[6] Abbasi, H. R., Sharifi Sedeh, E., Pourrahmani, H., & Mohammadi, M. H. (2020). Shape optimization of segmental porous baffles for enhanced thermohydraulic performance of shell-and-tube heat exchanger. *Applied Thermal Engineering*, 180. https://doi.org/10.1016/j.applthermaleng.2020.115835

[7] Wang, S., Xiao, J., Wang, J., Jian, G., Wen, J., & Zhang, Z. (2018). Application of response surface method and multi-objective genetic algorithm to configuration optimization of Shell-and-tube heat exchanger with fold helical baffles. *Applied Thermal Engineering*, 129, 512–520. https://doi.org/10.1016/j.applthermaleng.2017.10.039

[8] Appendix B Thermophysical Properties of Water. (2015). In *Drying Phenomena* (pp. 457–459). Wiley. https://doi.org/10.1002/9781118534892.app2

[9] Adam, N. M., Attia, O. H., Al-Sulttani, A. O., Mahmood, H. A., As'arry, A., & Md Rezali, K. A. (2020). Numerical Analysis for Solar Panel Subjected with an External Force to Overcome Adhesive Force in Desert Areas. CFD Letters,

12(9), 60–75. https://doi.org/10.37934/cfdl.12.9.6075
[10] Abbasian Arani, A. A., & Moradi, R. (2019). Shell and tube heat exchanger optimization using new baffle and tube configuration. *Applied Thermal Engineering*, 157, 113736. https://doi.org/10.1016/j.applthermaleng.2019.113736
[11] Tavakoli, M., & Soufivand, M. R. (2023). Performance evaluation criteria and entropy generation of hybrid nanofluid in a shell-and-tube heat exchanger with two different types of cross-sectional baffles. *Engineering Analysis with Boundary Elements*, 150, 272–284. https://doi.org/10.1016/j.enganabound.2023.01.024
[12] Adam, N. M., Attia, O. H., Al-Sulttani, A. O., Mahmood, H. A., As'arry, A., & Md Rezali, K. A. (2020). Numerical Analysis for Solar Panel Subjected with an External Force to Overcome Adhesive Force in Desert Areas. *CFD Letters*, 12(9), 60–75. https://doi.org/10.37934/cfdl.12.9.6075